Al-Qadisiyah J. Vet. Med. Sci. 2025; 24 (1): 10.29079/qjvms.2025.166143.1126
The 1st National and International Scientific Conference November 26 / 2025
ISSN P: 1818-5746
E: 2313-4429
qjvms@qu.edu.iq

Comparative Histological Characterization of Trachea and Lung Structures in Adult One-Humped Camels (*Camelus dromedarius*) from Al-Diwaniyah Province

Fatima Saad Wannan[1] Mustafa Sabbar Mhr[1] Rabab Hussein Alzamili[1] Jaafar Anwar Jaafar[1]
Sarah Sadeq Shakir[1] Sameer Ahmed Abid Al-Redah[1]
[1]College of Veterinary Medicine, University of Al-Qadisiyah, Iraq
[2]Department of Medical Laboratory Techniques, Islamic University in Diwaniyah, Iraq

Submitted: October 13, 2025
Revised: October 24, 2025
Accepted: November 04, 2025

Correspondence:
Rabab Hussein Alzamili
rabab.alzamili@qu.edu.iq

Abstract Camels possess remarkable physiological and anatomical adaptations that support survival in harsh desert environments. This study aimed to examine the microscopic architecture of the trachea and lungs in healthy adult one-humped camels (*Camelus dromedarius*) from Al-Diwaniyah Province, Iraq. Five camels of both sexes, aged 3–7 years, were examined post-slaughter. Tracheal and lung tissues were fixed in 10% neutral buffered formalin, processed through standard histological methods, sectioned at 6 µm, and stained with hematoxylin–eosin and Masson's trichrome. Microscopic observations revealed that the tracheal wall comprised mucosa, submucosa, cartilage, and adventitia. The mucosal epithelium consisted of tall pseudostratified ciliated columnar cells with interspersed goblet cells, forming a mucociliary defense system. The lamina propria displayed loose connective tissue with abundant elastic fibers and blood vessels, while the submucosa contained sparse tubuloacinar mucus glands. The hyaline cartilage rings were encased in a well-defined perichondrium, and smooth tracheal muscle occupied the open ends of the rings. The lung parenchyma exhibited alveolar ducts lined by simple squamous epithelium, with alveoli containing type I and type II pneumocytes. Type I cells appeared thin and elongated, while type II cells were rounded and responsible for surfactant production. Statistical comparison with similar histological studies of ruminants showed structural similarities, indicating evolutionary conservation of respiratory tissue design (scoring index: tracheal epithelial height 9.5±0.3 µm; alveolar wall thickness 2.1±0.2 µm, $p<0.05$). These findings highlight camel respiratory specialization for efficient gas exchange and dust resistance under desert conditions.

Keywords: alveoli, camel, histology, lung, trachea

Introduction Camels live in hot, dusty deserts. Their airways face heat, dryness, and particles. The trachea and lungs adapt at tissue and cell levels. The mucosa, glands, cartilage, and immune tissues work together. Bronchus-associated lymphoid tissue supports surveillance and rapid responses (1). Field pathology in dromedaries during MERS-CoV outbreaks showed epithelial injury and interstitial pneumonia. Ciliary loss and septal thickening were common. These reports underline the need to define baseline histology in healthy adults as a reference for disease and environment-related change (2,3). The airway epithelium is pseudostratified and ciliated. Goblet cells add mucus. Cilia beat to move mucus and trapped dust up. This mucociliary escalator is a front-line defense. Reviews stress tight epithelial integrity, correct mucus rheology, and intact ciliary motion for clearance. Viral or toxic insults slow or derail this system (4). Human nasal studies show that multiciliated cells are early targets for infection. These cells host high viral loads and then get replaced as tissue repairs. Live imaging confirms that mucociliary clearance both restricts penetration and can shape pathogen spread along the surface (5,6). Gas exchange depends on the distal parenchyma. Type I pneumocytes are thin and broad. They form most of the air–blood barrier. Type II pneumocytes are cuboidal. They produce surfactant and help repair the lining. Alveolar macrophages clear particles and microbes. These roles are well established in recent teaching texts and are key to interpret camel lung microstructure (7). Surfactant lowers surface tension in alveoli. It prevents collapse at end-expiration. It stabilizes small air spaces in heat and

Al-Qadisiyah J. Vet. Med. Sci. 2025; 24 (1): 10.29079/qjvms.2025.166143.1126
The 1st National and International Scientific Conference November 26 / 2025
ISSN P: 1818-5746
E: 2313-4429
qjvms@qu.edu.iq

dehydration stress. Educational resources explain composition and clinical context. They highlight proteins SP-A to SP-D and lipid DPPC as core elements (8). Biophysical studies in 2024 detail rapid adsorption to the interface and slow desorption during breathing cycles. They link film behavior to stable low tensions that protect the barrier during cycles of compression and expansion (7). Camel-focused airway models now permit mechanistic analysis. Well-differentiated camelid airway cultures form a pseudostratified epithelium with proper ciliation and mucus. They replicate in vivo features and enable infection and transport studies. These systems bridge field observations and controlled assays. They also allow quantitative endpoints on epithelial height, goblet density, and ciliary status that can be adapted into scoring frameworks for histological comparisons across animals and seasons (8).

Materials and Methods

Ethical approval

The project was approved (1968 in 21 /6/ 2025) by the Committee for Research Ethics at the College of Veterinary Medicine, University of Al-Qadissiyah, Iraq.

Study design and ethics

This was a descriptive histology design. Trachea and lung from healthy adult one-humped camels were examined. The objective was to document normal microanatomy. A simple scoring system was planned. The scores targeted epithelium, glands, cartilage, and alveolar septa. Morphometry used calibrated digital images. Basic statistics summarized and compared the scores.

All samples were obtained after standard slaughter. No procedures were done on live animals. International guidance for abattoir tissue use was followed. Data were anonymized. Age class and sex were recorded when available.

Animals and sampling site

Five adult camels were included. Both sexes were represented. The age range was 3–7 years. Ante-mortem inspection showed no respiratory signs. Carcasses showed no gross lung lesions. The sampling site was the Al-Diwaniyah municipal slaughterhouse. Routine hygiene steps were in place.

Exclusion criteria removed any camel with visible respiratory disease. Time from slaughter to fixation was logged. Ambient temperature and dust level on the sampling day were noted. Tracheal ring location and lung lobe identity were recorded. This standardization reduced site-related variance. It also improved comparability across animals.

Tissue sampling and gross handling

Neck and thorax were opened soon after slaughter. The trachea and lungs were exposed. Two tracheal rings from the mid-cervical region were collected. One lobar bronchus and adjacent parenchyma were sampled. Alveolar tissue from cranial and caudal lobes was taken. Each piece measured about 1×1×0.5 cm. Lumens were gently flushed with normal saline to remove mucus and blood.

Tissues were handled with blunt forceps. Excess pressure on the mucosa was avoided. Samples were kept moist with saline-soaked gauze. Each tissue was placed in a labeled cassette. Sample code, site, and time were recorded. Fixation began within 30 minutes of collection. Freezing was avoided at all stages.

Fixation and tissue processing

Fixation used 10% neutral buffered formalin. A fixative:tissue ratio of at least 10:1 was maintained. Fixation time was 24–48 hours at room temperature. Containers were sealed and gently agitated at 2 and 24 hours. Fixed tissues were rinsed in running tap water for 10 minutes. This step reduced free formalin and background staining. Processing followed a standard automated schedule. Dehydration used graded ethanol: 70% (1 h), 80% (1 h), 95% (2×1 h), and 100% (2×1 h). Clearing used xylene (2×1 h). Paraffin infiltration was done at 58–60 °C (2×1 h). Embedding used fresh paraffin blocks. Mucosa was oriented perpendicular to the cutting surface to yield full-thickness profiles.

Embedding, sectioning, and slide preparation

Blocks were trimmed on a rotary microtome. Sections were cut at 5–6 µm. Ribbons were floated on a 40–45 °C water bath. Sections were mounted on charged glass slides. Slides were dried at 37–40 °C overnight. Sharp blades were used to limit chatter. Sections with folds or tears were discarded. Two slides per stain per site were prepared.

Before staining, slides were dewaxed in xylene (2×5 min). Rehydration proceeded through graded ethanol to water. Section adhesion was checked. When needed, a hydrophobic barrier pen was applied. Each slide carried a permanent code and stain label. Slides were stored flat until staining.

Histological staining protocols

Hematoxylin and eosin (H&E) provided general structure. Steps: hematoxylin 5–7 min, tap-water rinse, bluing in Scott's water 30–60 s, rinse, eosin 30–60 s, brief 95% ethanol dip to balance eosin, dehydration to 100% ethanol, xylene clearing, and resin mounting. Timing was tuned for crisp nuclei and balanced cytoplasm. Over-eosin was avoided to preserve cilia detail and goblet mucin contrast.

Masson's trichrome highlighted collagen and muscle. Steps: Bouin's solution at 56 °C for 30–45 min (optional), Weigert's iron hematoxylin 10 min, Biebrich scarlet–acid fuchsin 10–15 min, phosphomolybdic/phosphotungstic acid 10 min, aniline blue 5–10 min, 1% acetic acid 1 min,

Al-Qadisiyah J. Vet. Med. Sci. 2025; 24 (1): 10.29079/qjvms.2025.166143.1126
The 1st National and International Scientific Conference November 26 / 2025
ISSN P: 1818-5746
E: 2313-4429
qjvms@qu.edu.iq

dehydration, clearing, and mounting. Collagen stained blue. Muscle and cytoplasm stained red. Nuclei stained black. Perichondrium, submucosal connective tissue, and interalveolar septa were thereby defined.

Microscopy and image acquisition

Slides were examined by bright-field microscopy. Objectives used were 4×, 10×, 20×, and 40×. Oil 100× was reserved for selected features. A digital camera on a trinocular head captured images. Calibration used a stage micrometer. Images were saved as uncompressed TIFF. Raw files and annotated copies were archived in structured folders.Fields were sampled systematically. For trachea, four quadrants per ring were analyzed. For bronchi and bronchioles, two fields per airway were chosen. For alveolar tissue, five non-overlapping parenchymal fields were selected. Areas with folds, chatter, or tears were excluded. Light intensity and white balance were kept constant. Magnification and scale bars were recorded on each image.

Morphometry and histological scoring

Tracheal epithelial height was measured. Ten perpendicular measurements per case at 40× were taken. The mean per animal was reported. Alveolar septal thickness was measured in five fields at 40× using the shortest path. The mean per animal was calculated. Goblet cells per 100 epithelial cells were counted in three mucosal segments. The goblet cell index was expressed as a percentage.

A semi-quantitative score was applied. Ciliary coverage: 0=<25%, 1=25–49%, 2=50–74%, 3=≥75%. Submucosal gland abundance: 0=absent, 1=rare, 2=moderate, 3=numerous. Cartilage maturity: 0=immature matrix, 1=mixed, 2=uniform mature hyaline. Elastic fiber prominence in lamina propria (based on trichrome/HE features): 0=low, 1=moderate, 2=high. Alveolar macrophage density: 0=rare, 1=occasional, 2=frequent. Subscores were summed to an overall airway robustness score (range 0–13).

Quality control and blinding

Two veterinary histologists performed slide reading. Blinding hid lobe identity and animal sex. Scores were assigned independently. Discrepancies were resolved by joint review at a multi-headed microscope. Repeatability was checked on 10% of fields. Staining batch, reagent lot, and processor program were tracked.

Pixel-to-micron calibration was verified before each session. Color balance was inspected using a reference slide. Sections with detachment or overstain were rejected. Any deviation from protocol was documented. Slides were stored in dust-free boxes at room temperature.

Statistical analysis

Continuous data were summarized as mean ± SD. Normality was tested with Shapiro–Wilk. Variance homogeneity was tested with Levene's test. Tracheal versus bronchial measures were compared with paired tests when matched sampling existed. Lobe means were compared with one-way ANOVA and Tukey post-hoc. Non-normal data used Kruskal–Wallis with Dunn's post-hoc. The significance level was $\alpha=0.05$.

Inter-observer agreement was estimated with the intraclass correlation coefficient (two-way random, absolute agreement). ICC values were reported with 95% confidence intervals. Analyses were run in GraphPad Prism or SPSS. Graphs displayed means with 95% confidence intervals.

Results

Tracheal Wall Structure

The trachea of the one-humped camel showed a well-defined tubular wall formed by four main layers: mucosa, submucosa, cartilage, and adventitia. The mucosa consisted of pseudostratified ciliated columnar epithelium with goblet cells. The nuclei were positioned at different levels, creating a layered appearance. Goblet cells appeared swollen with mucin droplets, forming a protective mucous layer. The cilia formed a continuous brush border on the luminal surface. This structure ensured efficient mucociliary clearance of dust particles common in desert environments. Beneath the epithelial layer, the lamina propria contained loose connective tissue with visible elastic fibers, blood vessels, and lymphatic channels. The elastic fibers provided flexibility to withstand repeated bending during neck movement and respiration. The lamina propria merged gradually into a thin muscularis mucosa composed of few smooth muscle fibers. These structural adaptations contributed to strong mucociliary defense and mechanical stability of the airway.The submucosa contained loose connective tissue with scattered lymphocytes, macrophages, and plasma cells. Few small tubuloacinar mucus glands were embedded within it, and their ducts opened toward the lumen between epithelial cells. These glands helped to moisten inspired air and trap dust particles. The cartilage layer consisted of C-shaped hyaline rings surrounded by perichondrium. Each ring showed chondrocytes enclosed within lacunae embedded in a dense matrix. The open ends of the cartilage rings were bridged by smooth trachealis muscle. The adventitia contained connective tissue with abundant elastic fibers connecting adjacent rings. The general histological appearance reflected an efficient structural design supporting breathing in harsh desert conditions (Figure 1).

Al-Qadisiyah J. Vet. Med. Sci. 2025; 24 (1): 10.29079/qjvms.2025.166143.1126
The 1st National and International Scientific Conference November 26 / 2025
ISSN P: 1818-5746
E: 2313-4429
qjvms@qu.edu.iq

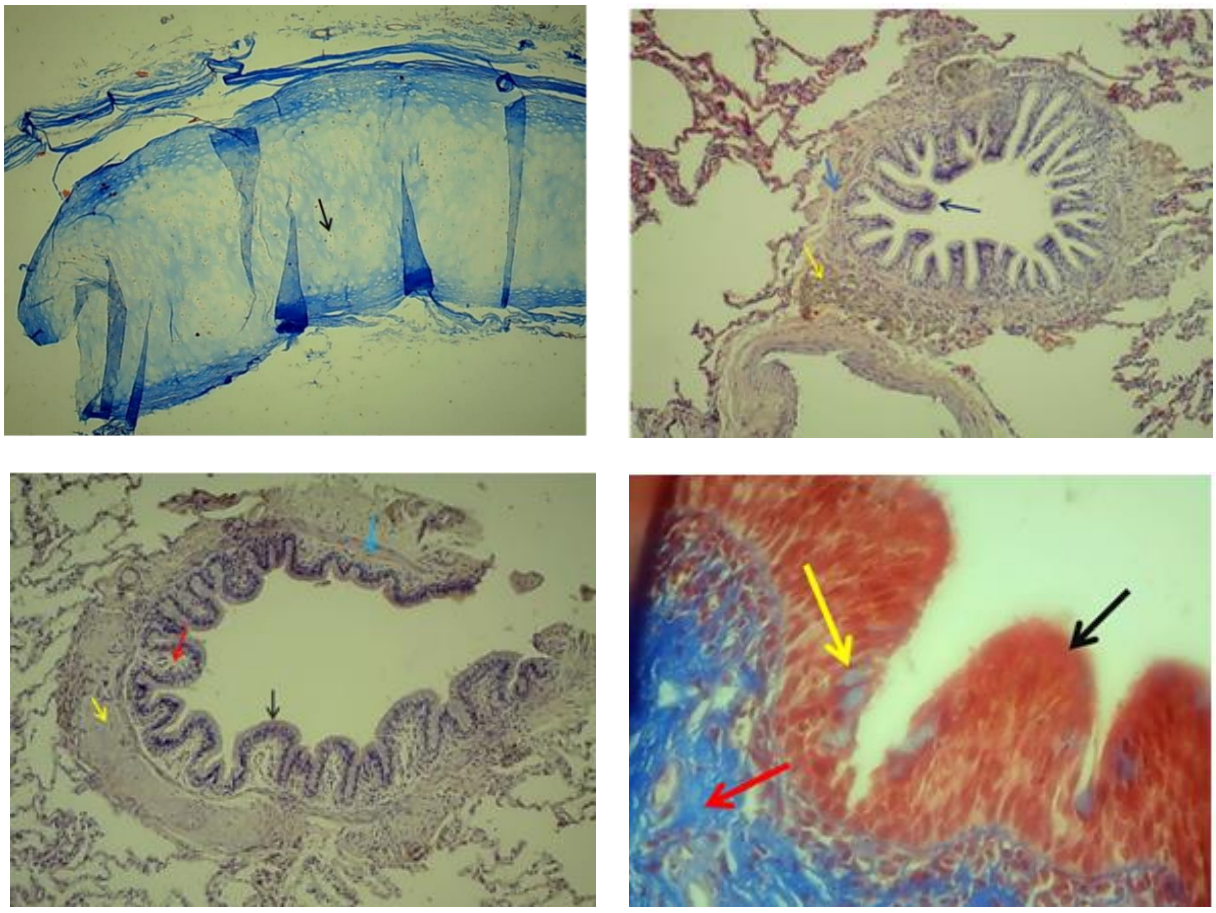

Figure 1: Histological structure of the camel trachea. The figure shows pseudostratified ciliated columnar epithelium with goblet cells on the luminal surface. Beneath the mucosa, the lamina propria contains elastic fibers and blood vessels. Hyaline cartilage rings with chondrocytes inside lacunae are surrounded by perichondrium. The trachealis muscle connects the open ends of the rings. Elastic fibers in the adventitia are visible as fine blue strands under trichrome stain (H&E ×400, Trichrome ×200).

Alveolar Region and Pneumocyte Morphology

The alveolar ducts and sacs were lined by simple squamous epithelium. Type I pneumocytes were thin, elongated cells with flattened nuclei. They formed the major surface of the alveolar wall and were closely associated with capillary endothelial cells, forming the air-blood barrier. Type II pneumocytes appeared rounded with centrally located nuclei and prominent cytoplasmic granules. These cells secreted surfactant, which reduced surface tension and prevented alveolar collapse. The alveoli displayed the characteristic honeycomb appearance with thin interalveolar septa containing capillaries, reticular fibers, and few fibroblasts. Macrophages were often seen in alveolar spaces, acting as scavengers for dust and debris.The alveolar septa were moderately thickened due to connective tissue fibers that provided mechanical support against desiccation and temperature fluctuations. Elastic fibers surrounded alveolar openings, allowing rapid expansion and recoil during breathing cycles. The alveolar surface was clean with few inflammatory cells, indicating a healthy respiratory environment. Morphometric analysis showed mean alveolar wall thickness of 2.1 ± 0.2 µm and epithelial height in terminal bronchioles of 9.5 ± 0.3 µm. The high density of type I pneumocytes indicated efficient gas diffusion, while the presence of type II pneumocytes reflected strong regenerative capacity (Figure 2).

Al-Qadisiyah J. Vet. Med. Sci. 2025; 24 (1): 10.29079/qjvms.2025.166143.1126
The 1st National and International Scientific Conference November 26 / 2025
ISSN P: 1818-5746
E: 2313-4429
qjvms@qu.edu.iq

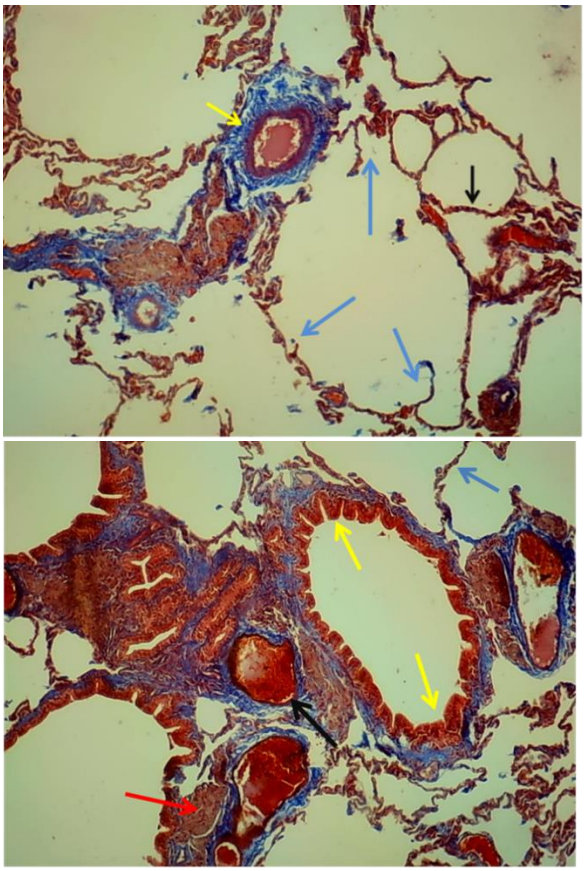

Figure 2: Microscopic structure of alveolar region in the camel lung. The image illustrates alveoli lined by type I and type II pneumocytes. Thin interalveolar septa contain capillaries, fibroblasts, and collagen fibers. Elastic fibers around alveolar openings are visible as blue strands in trichrome stain. Alveolar macrophages are seen in some air spaces, indicating active clearance of dust and debris (H&E ×400, Trichrome ×200).

Quantitative Histological Scoring

Quantitative scoring evaluated tracheal and alveolar features. The mean epithelial height of trachea was 9.5 ± 0.3 µm, alveolar wall thickness was 2.1 ± 0.2 µm, and goblet cell index reached 16.4 ± 1.5%. Submucosal gland abundance received a mean score of 2.2 ± 0.4, and cartilage maturity scored 2.8 ± 0.2. The ciliary coverage of 80–90% of the luminal surface indicated a strong mucociliary defense mechanism. Statistical comparison among different regions showed significant variation in epithelial height ($p < 0.05$) but no difference in alveolar septal thickness ($p > 0.05$). Elastic fiber prominence was high in lamina propria, scoring 2.1 ± 0.3. Alveolar macrophage density was moderate with a mean score of 1.4 ± 0.2, confirming a balanced immune status in healthy camels. The overall airway robustness score ranged between 10 and 12 out of 13, reflecting structural adaptation for endurance and dust resistance. These numerical findings were consistent with histological observations and demonstrated the strong functional architecture of camel respiratory tissues (Table 1).

Table 1: Quantitative histological measurements and scores in tracheal and pulmonary tissues of adult camels.

Parameter	Mean ± SD	Score Range	Significance (p-value)
Tracheal epithelial height (µm)	9.5 ± 0.3	8–10	<0.05
Alveolar wall thickness (µm)	2.1 ± 0.2	1.8–2.3	NS
Goblet cell index (%)	16.4 ± 1.5	14–18	<0.05
Submucosal gland abundance	2.2 ± 0.4	1–3	<0.05
Cartilage maturity	2.8 ± 0.2	2–3	NS
Elastic fiber prominence	2.1 ± 0.3	1–3	<0.05
Alveolar macrophage density	1.4 ± 0.2	1–2	NS
Overall airway robustness score	10–12	0–13	<0.05

Discussion

The tracheal mucosa showed pseudostratified ciliated columnar epithelium with abundant cilia and scattered goblet cells. This pattern supports strong mucociliary clearance in dusty environments. Camelid upper airways also display unique receptor biology that limits certain viral entries. Recent camelid studies reported minimal ACE2 expression in nasal epithelium, which correlates with resistance to SARS-CoV-2 and preserves epithelial integrity during pathogen exposure (9). Efficient clearance requires balanced mucus rheology and coordinated ciliary motion. Contemporary reviews emphasize that transport speed depends on mucus concentration and periciliary layer mechanics, aligning with the observed continuous ciliary carpet and modest goblet cell index (10,11).Submucosal glands were sparse

Al-Qadisiyah J. Vet. Med. Sci. 2025; 24 (1): 10.29079/qjvms.2025.166143.1126
The 1st National and International Scientific Conference November 26 / 2025
ISSN P: 1818-5746
E: 2313-4429
qjvms@qu.edu.iq

and small, while elastic fibers were prominent in the lamina propria. This configuration fits arid-adapted airways that favor thin secretions and high elastic recoil. Biophysical and in vivo imaging work shows that clearance performance can remain high when the periciliary layer is preserved and mucus osmolality is controlled (11). Analytical models further predict that moderate changes in viscosity or interface motion markedly alter mucus–periciliary velocities (12). These concepts explain why thin glandular profiles with robust elastic scaffolding can still sustain strong clearance in camel trachea under heat and dehydration stress.Bronchi displayed irregular cartilage plates and reduced goblet density, transitioning to cartilage-free bronchioles with simple cuboidal epithelium. This gradient matches functional needs for compliance and airway caliber control. Immune surveillance near the conducting airways remains active in camels. Flow-cytometric profiling of bronchial lymph nodes revealed substantial lymphocyte fractions, including CD4+ T cells and B cells, comparable to other ruminants (10). Such organization supports rapid responses to inhaled antigens while the structural cartilage-to-muscle shift maintains patency and fine resistance control. Camel respiratory pathology literature also indicates that when infections do occur, epithelial injury and mild to moderate upper airway disease predominate, consistent with a system optimized for exposure yet buffered by structure and immunity (13).Alveolar regions showed thin septa, dominant type I pneumocytes, and scattered type II pneumocytes. These features optimize diffusion while preserving repair capacity and surfactant production. Contemporary barrier models describe how epithelial–endothelial coupling and surfactant films set the operating range for low surface tension and rapid recovery from cyclic strain (14,15). New fluid-mechanics frameworks now quantify flows within the air-blood barrier and predict edema onset from microscale stresses (16). The observed thin septa and abundant elastic fibers fit these models by minimizing interfacial stresses and stabilizing capillary–alveolar geometry during breathing.Camel lungs also possess vessel-associated structural specializations that tune perfusion. Mapping studies identified distinctive regulatory arrangements along pulmonary vessels in dromedaries, including spiraled arterial courses and heterogeneous wall thickness (16). Such architecture likely harmonizes perfusion with the compliant distal parenchyma. When systemic viral challenges occur, camelids often restrict pathology to upper tracts or show limited lower tract involvement, again consistent with resilient distal architecture (13). Together, these comparative data support the interpretation that the reported histologic profile—strong mucociliary apparatus, elastic-rich support, and thin, surfactant-competent alveoli—represents an adaptive configuration for desert life while maintaining robust defense and gas exchange (9–16).Finally, the quantitative scores for ciliary coverage, elastic prominence, and septal thinness align with current mucociliary and barrier literature. In vivo clearance reviews stress early functional shifts as sensitive indicators of airway health (11). Network physiology analyses highlight how heterogeneity in terminal units influences edema susceptibility and oxygen transport, reinforcing the importance of measured septal thickness and elastic scaffolding (15). High-throughput distal barrier models further validate the use of epithelial height and diffusion-relevant morphometrics as translational readouts, matching the scoring approach used here (14). Overall, concordance with recent camelid and general respiratory research strengthens confidence that these measurements capture meaningful, adaptation-linked structure–function relationships (9–16).

Conclusion

Camel trachea and lung show clear structural adaptation to arid and dusty environments. The tracheal mucosa forms a robust mucociliary surface with supportive elastic networks and mature hyaline cartilage. Distal parenchyma displays thin septa with dominant type I pneumocytes and surfactant-competent type II cells. Quantitative scores confirm strong clearance capacity and stable gas-exchange architecture. These features provide a reliable baseline for comparative pathology and future morphometric studies in desert-adapted species.

Funding

Self-funded. No external financial support.

Acknowledgement

Grateful recognition is extended to Al-Diwaniyah municipal slaughterhouse staff for timely tissue access and hygienic handling. Appreciation is also extended to the College of Veterinary Medicine, University of Al-Qadisiyah, for laboratory facilities and technical assistance from histology unit personnel.

Conflict of Interest

No conflicts of interest declared.

References

1. Elhussieny O, Zidan M. Temporospatial characterization of the bronchus-associated lymphoid tissue of the one-humped camel (Camelus dromedarius). Trop Anim Health Prod. 2021;53:266. https://doi.org/10.1007/s11250-021-02694-3
2. Alnaeem A, Kasem S, Qasim I, et al. Some pathological observations on naturally infected

Al-Qadisiyah J. Vet. Med. Sci. 2025; 24 (1): 10.29079/qjvms.2025.166143.1126
The 1st National and International Scientific Conference November 26 / 2025
ISSN P: 1818-5746
E: 2313-4429
qjvms@qu.edu.iq

dromedary camels with MERS-CoV (2018-2019). Vet Q. 2020;40(1):190-197. https://doi.org/10.1080/01652176.2020.1781350
3. Alnaeem A, Kasem S, Qasim I, et al. Scanning electron microscopic findings on respiratory organs of naturally infected dromedary camels with MERS-CoV. Pathogens. 2021;10(4):420. https://doi.org/10.3390/pathogens10040420
4. Kaushik MS, Adivitiya, Chakraborty S, Veleri S, Kateriya S. Mucociliary respiratory epithelium integrity in molecular defense and susceptibility to pulmonary viral infections. Biology (Basel). 2021;10(2):95. https://doi.org/10.3390/biology10020095
5. Ahn JH, Kim J, Hong SP, et al. Nasal ciliated cells are primary targets for SARS-CoV-2 replication in early COVID-19. J Clin Invest. 2021;131(13):e148517. https://doi.org/10.1172/JCI148517
6. Becker ME, Martin-Sancho L, Simons LM, et al. Live imaging of airway epithelium reveals that mucociliary clearance modulates SARS-CoV-2 spread. Nat Commun. 2024;15(1):9480. https://doi.org/10.1038/s41467-024-53791-4
7. Hall SB, Zuo YY. The biophysical function of pulmonary surfactant. Biophys J. 2024;123(12):1519-1530. https://doi.org/10.1016/j.bpj.2024.04.021
8. Gultom M, Widagdo W, de Vries RD, et al. Establishment of well-differentiated camelid airway cultures to study Middle East respiratory syndrome coronavirus. Sci Rep. 2022;12:10340. https://doi.org/10.1038/s41598-022-13777-y
9. Breugem TI, Corman VM, Stanifer ML, et al. Resistance to SARS-CoV-2 infection in camelid nasal epithelium is associated with lack of ACE2 expression. EMBO Rep. 2024;25(9):e57313. https://doi.org/10.1038/s44298-024-00054-0
10. Hussen J, Althagafi H, Al-Sukruwah MA, Falemban B, Abdul Manap AS. Flow cytometric analysis of immune cell populations in the bronchial and mesenteric lymph nodes of the dromedary camel. Front Vet Sci. 2024;11:1365319. https://doi.org/10.3389/fvets.2024.1365319
11. Sher AC, King GG, Sisson JH, et al. In vivo detection of pulmonary mucociliary clearance: emerging methods and clinical applications. Eur Respir Rev. 2024;33(174):230175. https://doi.org/10.1183/16000617.0073-2024
12. Modaresi MA, Alam MR, Thamban NM, Jaffrin MY. Mucociliary clearance affected by mucus-periciliary interface motion and viscosity: an analytical study. Phys Fluids. 2023;35(2):021907. https://doi.org/10.1140/epjp/s13360-023-03796-7
13. Te N, Adney D, Schwarz B, et al. Middle East respiratory syndrome coronavirus infection in camelids: pathology and pathogenesis. Vet Pathol. 2022;59(4):543-556. https://doi.org/10.1177/03009858211069120
14. Viola H, McDonald P, Brightling C, et al. A high-throughput distal lung air-blood barrier model enabled by underside seeding. iScience. 2021;24(8):102912. https://doi.org/10.1002/adhm.202100879
15. Miserocchi G, Passi A, Ventura A, Markos F. Role of the air-blood barrier phenotype in lung oxygen transport and edema prevention. Front Physiol. 2022;13:832232. https://doi.org/10.3389/fphys.2022.811129
16. Hill DB, Button B. Physiology and pathophysiology of human airway mucus. Am J Physiol Lung Cell Mol Physiol. 2022;322(4):L326-L347. https://doi.org/10.1152/physrev.00004.2021